Acta Mech. Sin. (2018) 34(2):371–380
https://doi.org/10.1007/s10409-017-0690-7

RESEARCH PAPER

Generalized mixed finite element method for 3D elasticity problems

Guanghui Qing[1] · **Junhui Mao**[1] · **Yanhong Liu**[1]

Received: 12 March 2017 / Revised: 20 April 2017 / Accepted: 10 May 2017 / Published online: 28 June 2017

Abstract Without applying any stable element techniques in the mixed methods, two simple generalized mixed element (GME) formulations were derived by combining the minimum potential energy principle and Hellinger–Reissner (H–R) variational principle. The main features of the GME formulations are that the common C_0-continuous polynomial shape functions for displacement methods are used to express both displacement and stress variables, and the coefficient matrix of these formulations is not only automatically symmetric but also invertible. Hence, the numerical results of the generalized mixed methods based on the GME formulations are stable. Displacement as well as stress results can be obtained directly from the algebraic system for finite element analysis after introducing stress and displacement boundary conditions simultaneously. Numerical examples show that displacement and stress results retain the same accuracy. The results of the noncompatible generalized mixed method proposed herein are more accurate than those of the standard noncompatible displacement method. The noncompatible generalized mixed element is less sensitive to element geometric distortions.

Keywords Minimum potential energy principle · Hellinger–Reissner (H–R) variational principle · Generalized variational principle · Generalized mixed element (GME) · Elasticity problem · Noncompatible mode

✉ Guanghui Qing
qingluke@126.com

[1] College of Aeronautical Engineering, Civil Aviation University of China, Tianjin 300300, China

1 Introduction

In standard finite element displacement methods, the displacements are usually computed first, then the stresses or/and strains are calculated by numerically differentiating, based upon the constitutive relations and compatible equations at element level, usually resulting in loss of accuracy. Meanwhile, the values of the strain component computed from different elements connected at a node are different. Consequently, a smoothing or recovery procedure for nodal stresses may be carried out over the local or whole finite element domain. The boundary nodal stresses obtained from such finite element analysis are inconsistent with the prescribed stresses in displacement methods [1,2].

For equilibrium finite element methods, stresses are equilibrated within the element and tractions are balanced at interelement boundaries. However, equilibrium methods have been found to have limited use in general-purpose computer codes because of their behavior without judicious choice of basis functions [2].

Numerous mathematical models result from physical problems in the form of systems of partial differential equations involving several physically disparate quantities that need to be approximated simultaneously. The finite element approximations of such problems are well known as mixed finite element methods. Generally, the dual variable is computed as a fundamental unknown in mixed methods. Early contributions towards mixed methods can be found in Refs. [3–10]. More recent developments can be found in Refs. [11–25]. As a class of numerical methods, mixed models are widely used in the field of fluid mechanics; For example, displacement models are impractical for the Stokes problem. For such problems, mixed methods represent the simplest and most direct alternative [25].

Several main advantages and disadvantages of mixed methods can be summarized as follows:

(1) Linear interpolation functions are often sufficient to give satisfactory results for practical applications. Boundary and interelement conditions can be represented properly, and no difficulties arise due to higher derivatives;
(2) The stress or strain variables, as the main design parameters of a structure, are the direct results of the finite element governing equation without requiring differentiation of displacements. This is also advantageous for physically nonlinear analysis, in which yield conditions etc. are expressed in terms of stresses [8,11];
(3) It is well known that, for nearly incompressible and incompressible materials, finite element computations based on the standard displacement formulation fail due to the onset of the locking phenomenon. Classical mixed formulations are a valid alternative to locking-affected methods, since they provide mathematical models capable of treating both compressible and incompressible elasticity problems in a unified framework [8,26];
(4) Compared with displacement methods, the mathematical theory of mixed methods is relatively complex. For mixed methods based on the Hellinger–Reissner (H–R) variational principle alone, stability is paramount. The stability of numerical results is related to the invertibility of the coefficient matrix of the finite element governing equation. A main drawback of mixed methods is the indefiniteness of the resulting system matrix [20]. It is not easy to construct a pair of finite elements for the displacement vector and symmetric stress tensor which satisfies the stability conditions of Brezzi's theory [4].

Some representative studies on mixed methods published in recent years should be mentioned here: Arnold and Winther [16] suggested some stable elements for a two-dimensional problem, while the corresponding method in three-dimensional space was first characterized by Adams and Cockburn [17], and thorough analyses of the finite elements were provided in Ref. [19]. The construction of these elements is not convenient for computer programs, since they are of high polynomial order, implying high cost even for the lowest-order scheme. A family of symmetric tensor-valued finite elements of arbitrary order was constructed using the tangential-displacement normal-normal-stress (TDNNS) formulation in Ref. [10]. However, the mathematical theory and the process of construction of the TDNNS formulation are not simple and not suitable for engineers.

No doubt, some open questions remain in connection with displacement methods, equilibrium methods, and mixed methods for two- or three-dimensional elasticity problems. For mixed methods, some questions of stable elements require further study.

The objective of this work is to propose two simple generalized mixed methods without any stable element schemes but with automatically stable numerical results.

2 Variational principles for elasticity

Consider a body under static loading. The body occupies the volume V. S is the surface of the body. $S = S_u \cup S_\sigma$, where S_u and S_σ are the segments of S where displacements and surface tractions are prescribed, respectively; the outward unit normal on S is denoted by $\boldsymbol{N} \equiv n_i$. Let ∇ be the gradient operator in the deformed body which, under the assumption of infinitesimal deformation, is indistinguishable from the deformed body.

We define the following: displacements $\boldsymbol{u} \equiv u_i$, strains $\boldsymbol{\varepsilon} \equiv \varepsilon_{ij}$, and stresses $\boldsymbol{\sigma} \equiv \sigma_{ij}$; $\boldsymbol{b} \equiv b_i$ as the body force in V; the surface tractions $\boldsymbol{T} \equiv T_i$, and the prescribed surface tractions $\overline{\boldsymbol{T}} \equiv \overline{T}_i$ on S_σ; the prescribed displacements $\overline{\boldsymbol{u}} \equiv \overline{u}_i$ on S_u.

Assuming the displacement boundary conditions $\boldsymbol{u} - \overline{\boldsymbol{u}} = 0$ is satisfied a priori for all variational principles in the following.

The minimum potential energy principle for elasticity problems has the form

$$\Pi_P = \int_V \left[\frac{1}{2}(\nabla \boldsymbol{u})^T \boldsymbol{C}(\nabla \boldsymbol{u}) - \boldsymbol{b}^T \boldsymbol{u}\right] dV - \int_{s_\sigma} \overline{\boldsymbol{T}}^T \boldsymbol{u}\, dS, \quad (1)$$

where $\boldsymbol{C}$ is the symmetric stiffness matrix of a material.

The H–R variational principle [27] for elasticity problems contains both displacement and stress fields

$$\Pi_{HR} = \int_V \left[-\frac{1}{2}\boldsymbol{\sigma}^T \boldsymbol{S}\boldsymbol{\sigma} + \boldsymbol{\sigma}^T(\nabla \boldsymbol{u}) - \boldsymbol{b}^T \boldsymbol{u}\right] dV - \int_{s_\sigma} \overline{\boldsymbol{T}}^T \boldsymbol{u}\, dS, \quad (2)$$

where $\boldsymbol{S} = \boldsymbol{C}^{-1}$ is the compliance matrix.

Like the H–R variational principle, there are also both displacement and stress fields in the generalized variational principle [28]. This principle can be expressed in the following form

$$\Pi_G = \Pi_{HR} + \int_V \lambda \left[\frac{1}{2}\boldsymbol{\sigma}^T \boldsymbol{S}\boldsymbol{\sigma} + \frac{1}{2}(\nabla \boldsymbol{u})^T \boldsymbol{C}(\nabla \boldsymbol{u}) - \boldsymbol{\sigma}^T(\nabla \boldsymbol{u})\right] dV. \quad (3)$$

It should be pointed out that Felippa [29,30] constructed a one-parameter family of mixed variational principles for linear elasticity in 1989. Equation (3) is such a one-parameter family of mixed variational principles.

Generally, we expect to take $0 \leqslant \lambda \leqslant 1$ in Eq. (3). Values of the parameter $\lambda < 0$ or $\lambda > 1$ are not of practical interest.

It is clear that, letting $\lambda = 0$, Eq. (3) becomes the H–R variational principle. Meanwhile, letting $\lambda = 1$, one obtains the minimum potential energy principle in Eq. (1).

Letting $\lambda = \frac{1}{2}$ yields

$$\begin{aligned}\Pi_{\mathrm{G}} = \int_V \Big[&-\frac{1}{4}\boldsymbol{\sigma}^{\mathrm{T}}\boldsymbol{S}\boldsymbol{\sigma} + \frac{1}{2}\boldsymbol{\sigma}^{\mathrm{T}}(\nabla\boldsymbol{u}) + \frac{1}{4}(\nabla\boldsymbol{u})^{\mathrm{T}}\boldsymbol{C}(\nabla\boldsymbol{u}) \\ &-\boldsymbol{b}^{\mathrm{T}}\boldsymbol{u}\Big]\mathrm{d}V - \int_{s_\sigma} \overline{\boldsymbol{T}}^{\mathrm{T}}\boldsymbol{u}\mathrm{d}S \\ = \frac{1}{2}&(\Pi_{\mathrm{P}} + \Pi_{\mathrm{HR}}). \end{aligned} \tag{4}$$

It is interesting that the generalized variational principle above is one-half of the sum of the minimum potential energy principle and H–R variational principle. Our practice shows that, indeed, only for $\lambda = 1/2$ can good accuracy and stability of the generalized mixed method be obtained.

Note that the H–R variational principle in Eq. (2) and generalized variational principle in Eq. (4) are the principles of stationarity. For the principles in Eqs. (2) and (4), the nonvariational constraint is the constitutive relations. The equilibrium equations, the tractions boundary condition can be satisfied a posteriori.

3 Element formulations

3.1 Compatible mixed element formulations

Without loss of generality, consider first an n-node compatible linear element for 3D problems. Both the displacement vector $\boldsymbol{u}$ and stress vector $\boldsymbol{\sigma}$ are expressed using the same shape functions

$$\boldsymbol{u} = \boldsymbol{N}_{\mathrm{q}}\boldsymbol{q}_{\mathrm{e}}, \tag{5}$$

where $\mathrm{Diag}(\boldsymbol{N}_{\mathrm{q}}) = [\boldsymbol{N}_{\mathrm{e}}, \boldsymbol{N}_{\mathrm{e}}, \boldsymbol{N}_{\mathrm{e}}]^{\mathrm{T}}, \boldsymbol{N}_{\mathrm{e}} = [N_1, N_2, \ldots, N_n]$, $\boldsymbol{q}_{\mathrm{e}} = [\boldsymbol{u}_{1\mathrm{e}}, \boldsymbol{u}_{2\mathrm{e}}, \boldsymbol{u}_{3\mathrm{e}}]^{\mathrm{T}}$.

$$\boldsymbol{\sigma} = \boldsymbol{N}_{\mathrm{p}}\boldsymbol{p}_{\mathrm{e}} = \begin{bmatrix} \boldsymbol{N}_{\mathrm{q}} & \boldsymbol{0} \\ \boldsymbol{0} & \boldsymbol{N}_{\mathrm{q}} \end{bmatrix} \begin{pmatrix} \boldsymbol{p}_{\mathrm{oe}} \\ \boldsymbol{p}_{\mathrm{ie}} \end{pmatrix}, \tag{6}$$

where $\mathrm{Diag}(\boldsymbol{N}_{\mathrm{p}}) = [\boldsymbol{N}_{\mathrm{e}}, \boldsymbol{N}_{\mathrm{e}}, \boldsymbol{N}_{\mathrm{e}}, \boldsymbol{N}_{\mathrm{e}}, \boldsymbol{N}_{\mathrm{e}}, \boldsymbol{N}_{\mathrm{e}}]^{\mathrm{T}}$; $\boldsymbol{p}_{\mathrm{e}} = [\boldsymbol{p}_{\mathrm{oe}}, \boldsymbol{p}_{\mathrm{ie}}]^{\mathrm{T}} = [\boldsymbol{\sigma}_{13\mathrm{e}}, \boldsymbol{\sigma}_{23\mathrm{e}}, \boldsymbol{\sigma}_{33\mathrm{e}}, \boldsymbol{\sigma}_{11\mathrm{e}}, \boldsymbol{\sigma}_{22\mathrm{e}}, \boldsymbol{\sigma}_{12\mathrm{e}}]^{\mathrm{T}}$.

Let $N_i = \frac{1}{8}(1+\zeta_i\zeta)(1+\eta_i\eta)(1+\xi_i\xi)$, $i = 1, 2, \ldots, 8$, in Eqs. (5) and (6), thus $\boldsymbol{N}_{\mathrm{q}}$ is the 24×24 shape function matrix.

It is well known that, inserting Eqs. (5) and (6) into Eq. (2) and performing the energy integration, one obtains the discrete form of the H–R variational principle

$$\begin{aligned}\Pi_{\mathrm{HR}}(\boldsymbol{p}_{\mathrm{e}}, \boldsymbol{q}_{\mathrm{e}}) = \sum_{i=1}^{n} \Big[&-\frac{1}{2}\boldsymbol{p}_{\mathrm{e}}^{\mathrm{T}}\boldsymbol{K}_{\mathrm{pp}}^{(i)}\boldsymbol{p}_{\mathrm{e}} + \boldsymbol{p}_{\mathrm{e}}^{\mathrm{T}}\boldsymbol{K}_{\mathrm{pq}}^{(i)}\boldsymbol{q}_{\mathrm{e}} \\ &-\left(\boldsymbol{f}_{\mathrm{q}}^{(i)}\right)^{\mathrm{T}}\boldsymbol{q}_{\mathrm{e}}\Big], \end{aligned} \tag{7}$$

in which $\boldsymbol{K}_{\mathrm{pp}}^{(i)} = \int_{V_i} \boldsymbol{N}_{\mathrm{p}}^{\mathrm{T}}\boldsymbol{S}\boldsymbol{N}_{\mathrm{p}}\mathrm{d}V$ is a symmetric matrix of an element, $\boldsymbol{K}_{\mathrm{pq}}^{(i)} = \int_{V_i} \boldsymbol{N}_{\mathrm{q}}^{\mathrm{T}}(\nabla\boldsymbol{N}_{\mathrm{q}})\mathrm{d}V$ is a rectangular matrix, $\boldsymbol{f}_{\mathrm{q}}^{(i)} = \int_{V_i} \boldsymbol{N}_{\mathrm{q}}^{\mathrm{T}}\boldsymbol{b}\mathrm{d}V + \int_{S_{\sigma i}} \boldsymbol{N}_{\mathrm{q}}^{\mathrm{T}}\overline{\boldsymbol{T}}\mathrm{d}S$ is the load vector of an element; $\sum$ implies the summation of all individual elements.

In what follows, the superscript "i" will be dropped for clarity.

Consider $\boldsymbol{p}_{\mathrm{e}}$ and $\boldsymbol{q}_{\mathrm{e}}$ as independent variables. By $\delta\Pi_{\mathrm{HR}}(\boldsymbol{p}_{\mathrm{e}}, \boldsymbol{q}_{\mathrm{e}}) = 0$, one has two Euler–Lagrange (EL) equations

$$\begin{bmatrix} -\boldsymbol{K}_{\mathrm{pp}} & \boldsymbol{K}_{\mathrm{pq}} \\ \boldsymbol{K}_{\mathrm{pq}}^{\mathrm{T}} & \boldsymbol{0} \end{bmatrix} \begin{Bmatrix} \boldsymbol{p}_{\mathrm{e}} \\ \boldsymbol{q}_{\mathrm{e}} \end{Bmatrix} = \begin{Bmatrix} \boldsymbol{0} \\ \boldsymbol{f}_{\mathrm{q}} \end{Bmatrix}. \tag{8}$$

It can be seen that the classical formulation in Eq. (8) resulting from the H–R variational principle of various physical problems is symmetric, but it possesses zeros on the diagonal. Indeed, the coefficient matrix of Eq. (8) is non-positive definite. If stable elements [16,20,26] are not employed, it is very difficult to obtain stable solutions directly from Eq. (8).

3.2 Compatible displacement element formulations

In the same way, using Eq. (5), the discrete form of the minimum potential energy principle in Eq. (1) is

$$\Pi_{\mathrm{P}}(\boldsymbol{q}_{\mathrm{e}}) = \sum_{i=1}^{n} \left(\frac{1}{2}\boldsymbol{q}_{\mathrm{e}}^{\mathrm{T}}\boldsymbol{K}_{\mathrm{qq}}\boldsymbol{q}_{\mathrm{e}} - \boldsymbol{f}_{\mathrm{q}}^{\mathrm{T}}\boldsymbol{q}_{\mathrm{e}} \right), \tag{9}$$

in which $\boldsymbol{K}_{\mathrm{qq}} = \int_{V_i} (\nabla\boldsymbol{N}_{\mathrm{q}})^{\mathrm{T}}\boldsymbol{C}(\nabla\boldsymbol{N}_{\mathrm{q}})\mathrm{d}V$ is symmetric and positive definitive; Certainly, $\boldsymbol{f}_{\mathrm{q}} = \int_{V_i} \boldsymbol{N}_{\mathrm{q}}^{\mathrm{T}}\boldsymbol{b}\mathrm{d}V + \int_{S_{\sigma i}} \boldsymbol{N}_{\mathrm{q}}^{\mathrm{T}}\overline{\boldsymbol{T}}\mathrm{d}S$ is identical to $\boldsymbol{f}_{\mathrm{q}}$ in Eq. (7). As is well known, the EL equation corresponding to Eq. (9) is

$$\boldsymbol{K}_{\mathrm{qq}}\boldsymbol{q}_{\mathrm{e}} = \boldsymbol{f}_{\mathrm{q}}. \tag{10}$$

3.3 Compatible generalized mixed element formulations

It is of interest to see that adding Eq. (10) to the second equation of Eq. (8) yields

$$\begin{bmatrix} -\boldsymbol{K}_{\mathrm{pp}} & \boldsymbol{K}_{\mathrm{pq}} \\ \boldsymbol{K}_{\mathrm{pq}}^{\mathrm{T}} & \boldsymbol{K}_{\mathrm{qq}} \end{bmatrix} \begin{Bmatrix} \boldsymbol{p}_{\mathrm{e}} \\ \boldsymbol{q}_{\mathrm{e}} \end{Bmatrix} = \begin{Bmatrix} \boldsymbol{0} \\ 2\boldsymbol{f}_{\mathrm{q}} \end{Bmatrix}. \tag{11}$$

In the above equation, the coefficient matrix is not only symmetric, but also there are no zeros on the diagonal. This

is a main difference from Eq. (8). Equation (11) is termed the compatible generalized mixed element with 8 nodes (CGME8) for 3D problems in this work.

Certainly, Eq. (11) can be proved by the generalized variational principle in Eq. (4). Using Eqs. (5) and (6), the discrete form of Eq. (4) can be written as

$$\Pi_{\mathrm{G}}(\boldsymbol{p}_{\mathrm{e}},\boldsymbol{q}_{\mathrm{e}})=\sum\Big(-\frac{1}{4}\boldsymbol{p}_{\mathrm{e}}^{\mathrm{T}}\boldsymbol{K}_{\mathrm{pp}}\boldsymbol{p}_{\mathrm{e}}+\frac{1}{2}\boldsymbol{p}_{\mathrm{e}}^{\mathrm{T}}\boldsymbol{K}_{\mathrm{pq}}\boldsymbol{q}_{\mathrm{e}}+\frac{1}{4}\boldsymbol{q}_{\mathrm{e}}^{\mathrm{T}}\boldsymbol{K}_{\mathrm{qq}}\boldsymbol{q}_{\mathrm{e}}-\boldsymbol{f}_{\mathrm{q}}^{\mathrm{T}}\boldsymbol{q}_{\mathrm{e}}\Big). \tag{12}$$

In Eq. (12), the integral expressions of $\boldsymbol{K}_{\mathrm{pp}}$, $\boldsymbol{K}_{\mathrm{pq}}$, and $\boldsymbol{f}_{\mathrm{q}}$ are the same as those in Eq. (7), respectively; the integral expression $\boldsymbol{K}_{\mathrm{qq}}$ is identical to the $\boldsymbol{K}_{\mathrm{qq}}$ in Eq. (9).

Taking the variation of Eq. (12) with respect to variables $\boldsymbol{p}_{\mathrm{e}}$ and $\boldsymbol{q}_{\mathrm{e}}$ leads immediately to Eq. (11).

The summation of Eq. (11) on all elements gives a novel algebraic system for finite element analysis

$$\begin{bmatrix}-\boldsymbol{K}_{11} & \boldsymbol{K}_{12}\\ \boldsymbol{K}_{12}^{\mathrm{T}} & \boldsymbol{K}_{22}\end{bmatrix}\begin{Bmatrix}\boldsymbol{p}\\ \boldsymbol{q}\end{Bmatrix}=\begin{Bmatrix}\boldsymbol{0}\\ 2\boldsymbol{f}\end{Bmatrix}, \tag{13}$$

where $\boldsymbol{K}_{11}=\sum\boldsymbol{K}_{\mathrm{pp}}$, $\boldsymbol{K}_{22}=\sum\boldsymbol{K}_{\mathrm{qq}}$, $\boldsymbol{K}_{12}=\sum\boldsymbol{K}_{\mathrm{pq}}$, $\boldsymbol{p}=\sum\boldsymbol{p}_{\mathrm{e}}$, $\boldsymbol{q}=\sum\boldsymbol{q}_{\mathrm{e}}$, and $\boldsymbol{f}=\sum\boldsymbol{f}_{\mathrm{q}}$.

In general, at system level, the whole coefficient matrix has a structure equivalent to that of an element. It is clear that the coefficient matrix of Eq. (13) is characterized by symmetry with respect to the stress and displacement variables of all nodes. Certainly, the coefficient matrix of Eq. (13) is invertible, which implies that its numerical results will be stable [26,31].

3.4 Noncompatible generalized mixed element formulations

On the basis of Refs. [32,33], for a noncompatible element, the element displacement $\boldsymbol{u}$ can be expressed as a sum of the compatible part $\boldsymbol{N}_{\mathrm{q}}\boldsymbol{q}_{\mathrm{e}}$ and the noncompatible part $\boldsymbol{N}_{\mathrm{r}}\boldsymbol{r}_{\mathrm{e}}$

$$\boldsymbol{u}=\boldsymbol{N}_{\mathrm{q}}\boldsymbol{q}_{\mathrm{e}}+\boldsymbol{N}_{\mathrm{r}}\boldsymbol{r}_{\mathrm{e}}. \tag{14}$$

Here, $\boldsymbol{N}_{\mathrm{r}}$ is the shape function matrix with respect to points within elements; $\boldsymbol{r}_{\mathrm{e}}$ is the displacement vector corresponding to points within elements.

In a similar way, substituting Eq. (14) into Eq. (1) results in

$$\Pi_{\mathrm{P}}(\boldsymbol{q}_{\mathrm{e}},\boldsymbol{r}_{\mathrm{e}})=\sum_{i=1}^{n}\Big(\frac{1}{2}\boldsymbol{q}_{\mathrm{e}}^{\mathrm{T}}\boldsymbol{K}_{\mathrm{qq}}\boldsymbol{q}_{\mathrm{e}}+\boldsymbol{q}_{\mathrm{e}}^{\mathrm{T}}\boldsymbol{K}_{\mathrm{qr}}\boldsymbol{r}_{\mathrm{e}}+\frac{1}{2}\boldsymbol{r}_{\mathrm{e}}^{\mathrm{T}}\boldsymbol{K}_{\mathrm{rr}}\boldsymbol{r}_{\mathrm{e}}-\boldsymbol{f}_{\mathrm{q}}^{\mathrm{T}}\boldsymbol{q}_{\mathrm{e}}-\boldsymbol{f}_{\mathrm{r}}^{\mathrm{T}}\boldsymbol{r}_{\mathrm{e}}\Big). \tag{15}$$

In Eq. (15), $\boldsymbol{K}_{\mathrm{qr}}=\boldsymbol{K}_{\mathrm{rq}}^{\mathrm{T}}=\int_{V_i}(\nabla\boldsymbol{N}_{\mathrm{q}})^{\mathrm{T}}\boldsymbol{C}(\nabla\boldsymbol{N}_{\mathrm{r}})\mathrm{d}V$, $\boldsymbol{K}_{\mathrm{rr}}=\boldsymbol{K}_{\mathrm{rr}}^{\mathrm{T}}=\int_{V_i}(\nabla\boldsymbol{N}_{\mathrm{r}})^{\mathrm{T}}\boldsymbol{C}(\nabla\boldsymbol{N}_{\mathrm{r}})\mathrm{d}V$, and $\boldsymbol{f}_{\mathrm{r}}=\int_{V_i}\boldsymbol{N}_{\mathrm{r}}^{\mathrm{T}}\boldsymbol{b}\mathrm{d}V+\int_{S_{\sigma_i}}\boldsymbol{N}_{\mathrm{r}}^{\mathrm{T}}\overline{\boldsymbol{T}}\mathrm{d}S$.

The result of the variation of Eq. (15) with respect to $\boldsymbol{r}_{\mathrm{e}}$ is given by

$$\boldsymbol{K}_{\mathrm{qr}}^{\mathrm{T}}\boldsymbol{q}_{\mathrm{e}}+\boldsymbol{K}_{\mathrm{rr}}\boldsymbol{r}_{\mathrm{e}}=\boldsymbol{f}_{\mathrm{r}}. \tag{16}$$

Here, $\boldsymbol{K}_{\mathrm{rr}}$ is an invertible matrix [32,33]. From this, one obtains

$$\boldsymbol{r}_{\mathrm{e}}=\boldsymbol{K}_{\mathrm{rr}}^{-1}\boldsymbol{f}_{\mathrm{r}}-\boldsymbol{K}_{\mathrm{rr}}^{-1}\boldsymbol{K}_{\mathrm{qr}}^{\mathrm{T}}\boldsymbol{q}_{\mathrm{e}}. \tag{17}$$

Eliminating $\boldsymbol{r}_{\mathrm{e}}$ in Eq. (15) using Eq. (17), the following EL equation can be derived from the new form of Eq. (15)

$$\mathcal{K}_{\mathrm{qq}}\boldsymbol{q}_{\mathrm{e}}=\boldsymbol{f}_{\mathrm{q}}-\boldsymbol{K}_{\mathrm{qr}}\boldsymbol{K}_{\mathrm{rr}}^{-1}\boldsymbol{f}_{\mathrm{r}}, \tag{18}$$

in which $\mathcal{K}_{\mathrm{qq}}=\boldsymbol{K}_{\mathrm{qq}}-\boldsymbol{K}_{\mathrm{qr}}\boldsymbol{K}_{\mathrm{rr}}^{-1}\boldsymbol{K}_{\mathrm{qr}}^{\mathrm{T}}$.

In a similar way, on substitution of Eqs. (6) and (14) into Eq. (2), the resulting noncompatible finite element functional has the form

$$\Pi_{\mathrm{HR}}(\boldsymbol{p}_{\mathrm{e}},\boldsymbol{q}_{\mathrm{e}},\boldsymbol{r}_{\mathrm{e}})=\sum_{i=1}^{n}\Big(-\frac{1}{2}\boldsymbol{p}_{\mathrm{e}}^{\mathrm{T}}\boldsymbol{K}_{\mathrm{pp}}\boldsymbol{p}_{\mathrm{e}}+\boldsymbol{p}_{\mathrm{e}}^{\mathrm{T}}\boldsymbol{K}_{\mathrm{pq}}\boldsymbol{q}_{\mathrm{e}}-\boldsymbol{f}_{\mathrm{q}}^{\mathrm{T}}\boldsymbol{q}_{\mathrm{e}}+\boldsymbol{p}_{\mathrm{e}}^{\mathrm{T}}\boldsymbol{K}_{\mathrm{pr}}\boldsymbol{r}_{\mathrm{e}}-\boldsymbol{f}_{\mathrm{r}}^{\mathrm{T}}\boldsymbol{r}_{\mathrm{e}}\Big). \tag{19}$$

Here, $\boldsymbol{K}_{\mathrm{pr}}=\boldsymbol{K}_{\mathrm{rp}}^{\mathrm{T}}=\int_{V_i}\boldsymbol{N}_{\mathrm{p}}^{\mathrm{T}}(\nabla\boldsymbol{N}_{\mathrm{r}})\mathrm{d}V$.

Using Eq. (17), one can also eliminate $\boldsymbol{r}_{\mathrm{e}}$ from the above equation to yield

$$\Pi_{\mathrm{HR}}(\boldsymbol{p}_{\mathrm{e}},\boldsymbol{q}_{\mathrm{e}})=\sum_{i=1}^{n}\Big(-\frac{1}{2}\boldsymbol{p}_{\mathrm{e}}^{\mathrm{T}}\mathcal{K}_{\mathrm{pp}}\boldsymbol{p}_{\mathrm{e}}+\boldsymbol{p}_{\mathrm{e}}^{\mathrm{T}}\mathcal{K}_{\mathrm{pq}}\boldsymbol{q}_{\mathrm{e}}-\boldsymbol{f}_{\mathrm{q}}^{\mathrm{T}}\boldsymbol{q}_{\mathrm{e}}+\boldsymbol{p}_{\mathrm{e}}^{\mathrm{T}}\boldsymbol{K}_{\mathrm{pr}}\boldsymbol{K}_{\mathrm{rr}}^{-1}\boldsymbol{f}_{\mathrm{r}}+\boldsymbol{f}_{\mathrm{r}}^{\mathrm{T}}\boldsymbol{K}_{\mathrm{rr}}^{-1}\boldsymbol{K}_{\mathrm{qr}}^{\mathrm{T}}\boldsymbol{q}_{\mathrm{e}}-\boldsymbol{f}_{\mathrm{r}}^{\mathrm{T}}\boldsymbol{K}_{\mathrm{rr}}^{-1}\boldsymbol{f}_{\mathrm{r}}\Big). \tag{20}$$

Here, $\mathcal{K}_{\mathrm{pp}}=\boldsymbol{K}_{\mathrm{pp}}$ and $\mathcal{K}_{\mathrm{pq}}=\boldsymbol{K}_{\mathrm{pq}}-\boldsymbol{K}_{\mathrm{pr}}\boldsymbol{K}_{\mathrm{rr}}^{-1}\boldsymbol{K}_{\mathrm{qr}}^{\mathrm{T}}$.

Considering the combination of the result of $\delta\Pi_{\mathrm{HR}}(\boldsymbol{p}_{\mathrm{e}},\boldsymbol{q}_{\mathrm{e}})=0$ of Eq. (20) with respect to $\boldsymbol{p}_{\mathrm{e}}$ and Eq. (18), one has

$$\begin{bmatrix}-\mathcal{K}_{\mathrm{pp}} & \mathcal{K}_{\mathrm{pq}}\\ \mathcal{K}_{\mathrm{pq}}^{\mathrm{T}} & \mathcal{K}_{\mathrm{qq}}\end{bmatrix}\begin{Bmatrix}\boldsymbol{p}_{\mathrm{e}}\\ \boldsymbol{q}_{\mathrm{e}}\end{Bmatrix}=\begin{Bmatrix}-\boldsymbol{K}_{\mathrm{pr}}\boldsymbol{K}_{\mathrm{rr}}^{-1}\boldsymbol{f}_{\mathrm{r}}\\ 2\boldsymbol{f}_{\mathrm{q}}-2\boldsymbol{K}_{\mathrm{qr}}\boldsymbol{K}_{\mathrm{rr}}^{-1}\boldsymbol{f}_{\mathrm{r}}\end{Bmatrix}. \tag{21}$$

It should be mentioned that, if the body force is ignored, the vectors $-\boldsymbol{K}_{\mathrm{pr}}\boldsymbol{K}_{\mathrm{rr}}^{-1}\boldsymbol{f}_{\mathrm{r}}$ and $-2\boldsymbol{K}_{\mathrm{qr}}\boldsymbol{K}_{\mathrm{rr}}^{-1}\boldsymbol{f}_{\mathrm{r}}$ on the right-hand side of Eq. (21) are close to zero. Indeed, the term $\boldsymbol{f}_{\mathrm{r}}^{\mathrm{T}}\boldsymbol{r}_{\mathrm{e}}$ in Eq. (15) can be omitted in the classical noncompatible

displacement methods [32,33]. For the same reason, we can also omit the last term $\boldsymbol{f}_{\mathrm{r}}^{\mathrm{T}}\boldsymbol{r}_{\mathrm{e}}$ from Eq. (19), and thus the terms $-\boldsymbol{K}_{\mathrm{pr}}\boldsymbol{K}_{\mathrm{rr}}^{-1}\boldsymbol{f}_{\mathrm{r}}$ and $-2\boldsymbol{K}_{\mathrm{qr}}\boldsymbol{K}_{\mathrm{rr}}^{-1}\boldsymbol{f}_{\mathrm{r}}$ from the right-hand side of Eq. (21).

Therefore, the simplified noncompatible generalized mixed element with 8 nodes (NCGME8) for 3D problems is given by

$$\begin{bmatrix} -\mathcal{K}_{\mathrm{pp}} & \mathcal{K}_{\mathrm{pq}} \\ \mathcal{K}_{\mathrm{pq}}^{\mathrm{T}} & \mathcal{K}_{\mathrm{qq}} \end{bmatrix} \begin{Bmatrix} \boldsymbol{p}_{\mathrm{e}} \\ \boldsymbol{q}_{\mathrm{e}} \end{Bmatrix} = \begin{Bmatrix} \boldsymbol{0} \\ 2\boldsymbol{f}_{\mathrm{q}} \end{Bmatrix}. \tag{22}$$

The algebraic system for the finite element analysis corresponding to Eq. (22) has the form

$$\begin{bmatrix} -\mathcal{K}_{11} & \mathcal{K}_{12} \\ \mathcal{K}_{12}^{\mathrm{T}} & \mathcal{K}_{22} \end{bmatrix} \begin{Bmatrix} \boldsymbol{p} \\ \boldsymbol{q} \end{Bmatrix} = \begin{Bmatrix} \boldsymbol{0} \\ \boldsymbol{f} \end{Bmatrix}, \tag{23}$$

where $\mathcal{K}_{11} = \sum \mathcal{K}_{\mathrm{pp}}$, $\mathcal{K}_{12} = \sum \mathcal{K}_{\mathrm{pq}}$, $\mathcal{K}_{22} = \sum \mathcal{K}_{\mathrm{qq}}$, and $\boldsymbol{f} = 2\sum \boldsymbol{f}_{\mathrm{q}}$.

4 Imposing boundary conditions

For common finite element problems with prescribed but nonzero values at various locations, one approach in practice is to add a large number or penalty term, for instance 10^{20}, to the leading diagonal of the stiffness matrix in the row corresponding to the prescribed value. The term in the same row of the right-hand side vector is then set to the prescribed value multiplied by the augmented stiffness coefficient [33].

Such a procedure is only successful if small terms are indeed very small relative to 10^{20}. Another prerequisite may be required, i.e., that the coefficient matrix of the algebraic system is a bandwidth matrix. Our practice shows that this procedure is not suitable for Eqs. (13) and (23), which involve known nonzero stress values (e.g., the prescribed surface tractions) since the submatrix $\boldsymbol{K}_{12}$ in Eq. (13) or $\mathcal{K}_{12}$ in Eq. (23) is not a zero matrix.

Let us assume that $\boldsymbol{\vartheta}$ refers to the known value vector with respect to nodes on the surface or edges, whose values are determined by the prescribed surface tractions $\overline{\boldsymbol{T}}$ on S_σ and the prescribed displacement $\overline{\boldsymbol{u}}$ on S_{u}.

Taking Eq. (23) as an example, interchanging rows and columns, it can be recast into the following form

$$\begin{bmatrix} -\hat{\mathcal{K}}_{11} & \hat{\mathcal{K}}_{12} & \hat{\mathcal{K}}_{13} \\ \hat{\mathcal{K}}_{12}^{\mathrm{T}} & \hat{\mathcal{K}}_{22} & \hat{\mathcal{K}}_{23} \\ \hat{\mathcal{K}}_{13}^{\mathrm{T}} & \hat{\mathcal{K}}_{23}^{\mathrm{T}} & \hat{\mathcal{K}}_{33} \end{bmatrix} \begin{Bmatrix} \hat{\boldsymbol{p}} \\ \hat{\boldsymbol{q}} \\ \boldsymbol{\vartheta} \end{Bmatrix} = \begin{Bmatrix} \boldsymbol{f}_1 \\ \boldsymbol{f}_2 \\ \boldsymbol{f}_3 \end{Bmatrix}, \tag{24}$$

where $\hat{\boldsymbol{p}}$ and $\hat{\boldsymbol{q}}$ are the unknown parameter vectors of nodal stresses and displacements, respectively; the new coefficient submatrices $\boldsymbol{f}_1$, $\boldsymbol{f}_2$, and $\boldsymbol{f}_3$ are the results of interchanging rows and columns of the coefficient matrix and the load vector $\left[\boldsymbol{0}, \boldsymbol{f}\right]^{\mathrm{T}}$, respectively.

Therefore, one has

$$-\hat{\mathcal{K}}_{11}\hat{\boldsymbol{p}} + \hat{\mathcal{K}}_{12}\hat{\boldsymbol{q}} = \boldsymbol{f}_1 - \hat{\mathcal{K}}_{13}\boldsymbol{\vartheta}, \tag{25a}$$

$$\hat{\mathcal{K}}_{12}^{\mathrm{T}}\hat{\boldsymbol{p}} + \hat{\mathcal{K}}_{22}\hat{\boldsymbol{q}} = \boldsymbol{f}_2 - \hat{\mathcal{K}}_{23}\boldsymbol{\vartheta}, \tag{25b}$$

$$\hat{\mathcal{K}}_{13}^{\mathrm{T}}\hat{\boldsymbol{p}} + \hat{\mathcal{K}}_{23}^{\mathrm{T}}\hat{\boldsymbol{q}} = \boldsymbol{f}_3 - \hat{\mathcal{K}}_{33}\boldsymbol{\vartheta}. \tag{25c}$$

Of course, Eq. (25c) is redundant. Consequently, the final governing equation for the solutions of unknown nodal displacements and stresses is

$$\begin{bmatrix} -\hat{\mathcal{K}}_{11} & \hat{\mathcal{K}}_{12} \\ \hat{\mathcal{K}}_{12}^{\mathrm{T}} & \hat{\mathcal{K}}_{22} \end{bmatrix} \begin{Bmatrix} \hat{\boldsymbol{p}} \\ \hat{\boldsymbol{q}} \end{Bmatrix} = \begin{Bmatrix} \boldsymbol{f}_1 - \hat{\mathcal{K}}_{13}\boldsymbol{\vartheta} \\ \boldsymbol{f}_2 - \hat{\mathcal{K}}_{23}\boldsymbol{\vartheta} \end{Bmatrix}. \tag{26}$$

The simple technique presented above for imposing stress and displacement boundary conditions is employed in our program. In the next section, numerical examples show that the boundary nodal stresses are consistent with the prescribed stresses on S_σ.

5 Numerical examples and discussion

5.1 A thick rectangular plate with simply supported edges

Consider a thick rectangular plate with in-plane dimensions $a = b = 1.0$ and total thickness $h = 0.10$ (Fig. 1). Here, we assume that the edges $x = 0, a$ and $y = 0, b$ are simply supported, and use material properties $E_{11} = 10E_{22} = 10E_{33}$, $G_{12} = G_{13} = 0.6E_{33}$, $G_{23} = 0.5E_{33}$, and $\nu_{12} = \nu_{13} = \nu_{23} = 0.25$. Uniform normal load of 1.0 is applied on the upper surface of the plate [34].

Using the symmetry about the x_1- and x_2-axes, only one-quarter of the plate (Fig. 1b) is analyzed with uniform meshes.

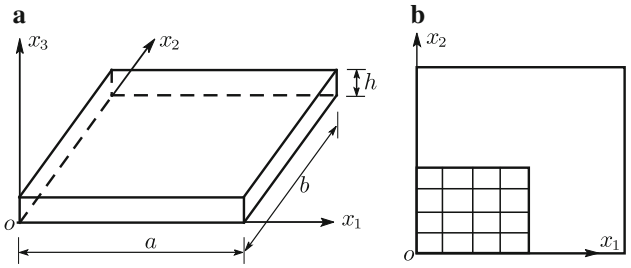

Fig. 1 A thick rectangular plate

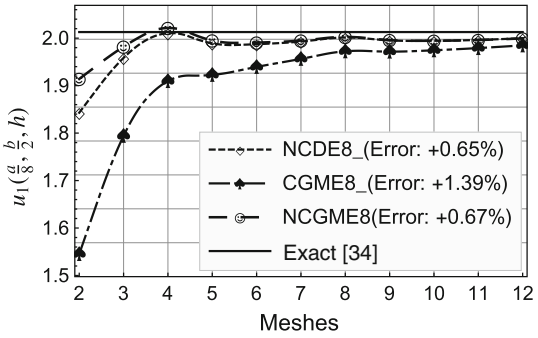

Fig. 2 Comparison of displacement $u_1\left(\frac{a}{8}, \frac{b}{2}, h\right)$

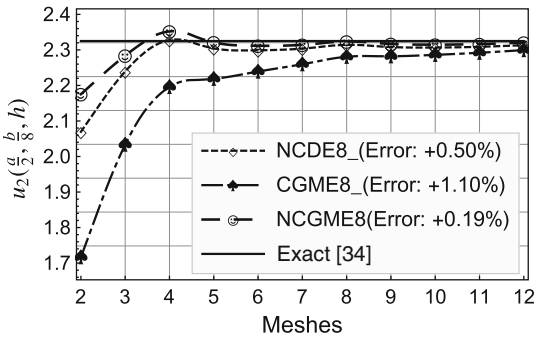

Fig. 3 Comparison of displacement $u_2\left(\frac{a}{2}, \frac{b}{8}, h\right)$

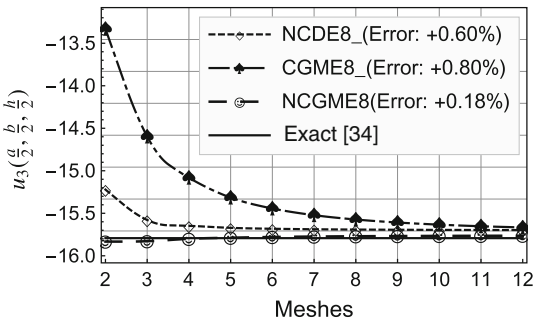

Fig. 4 Comparison of displacement $u_3\left(\frac{a}{2}, \frac{b}{2}, \frac{h}{2}\right)$

The convergence rate and accuracy of displacements and stresses at specific locations are depicted in Figs. 2–12. The results for the noncompatible displacement element with 8 nodes (NCDE8) were obtained using commercially available software ABAQUS®.

For Figs. 2–10, Table 1 presents the size of each mesh using the notation $l \times m$ for l subdivisions along the x_1-axis and m subdivisions along the x_2-axis with the same type of elements, with four subdivisions in the x_3 direction for all models.

On the basis of the results for the $12 \times 12 \times 4$ mesh, the errors presented in the legends to Figs. 2–10 were computed using the formula (Exact − Numerical)/Exact × 100 %.

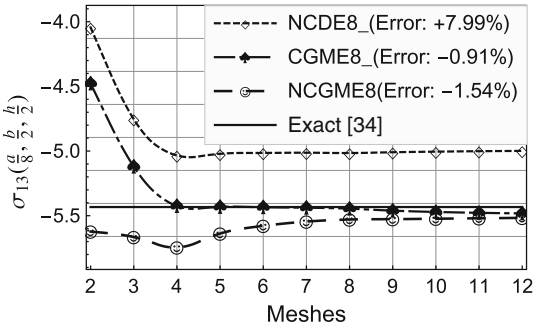

Fig. 5 Comparison of stress $\sigma_{13}\left(\frac{a}{8}, \frac{b}{2}, \frac{h}{2}\right)$

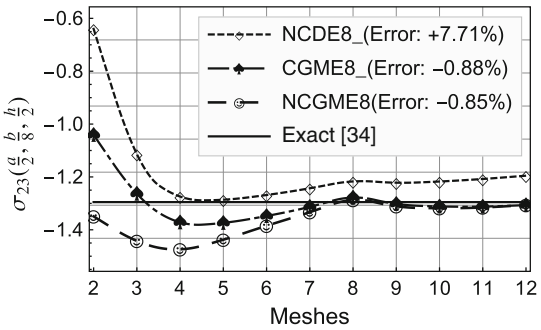

Fig. 6 Comparison of stress $\sigma_{23}\left(\frac{a}{2}, \frac{b}{8}, \frac{h}{2}\right)$

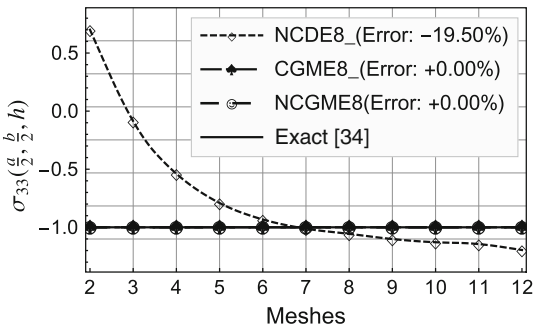

Fig. 7 Comparison of stress $\sigma_{33}\left(\frac{a}{2}, \frac{b}{2}, h\right)$

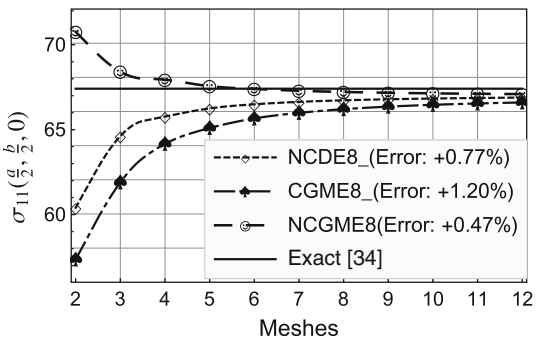

Fig. 8 Comparison of stress $\sigma_{11}\left(\frac{a}{2}, \frac{b}{2}, 0\right)$

In the present computer program, two Gauss quadrature points in each direction were employed for CGME8 and NCGME8.

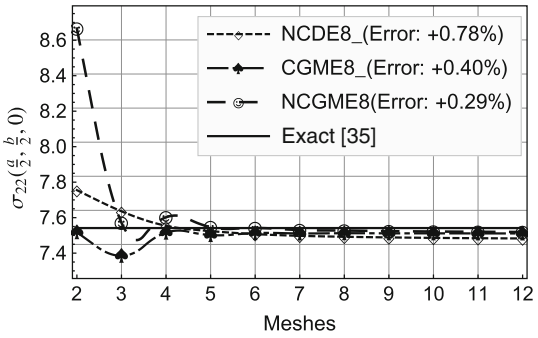

Fig. 9 Comparison of stress $\sigma_{22}\left(\frac{a}{2},\frac{b}{2},0\right)$

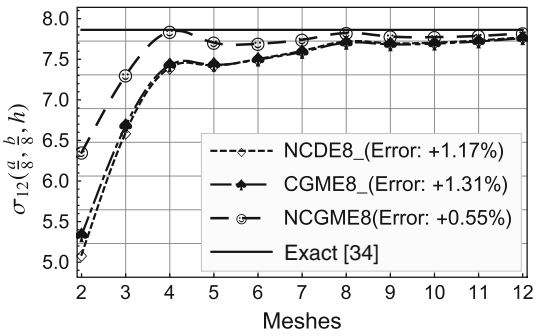

Fig. 10 Comparison of stress $\sigma_{12}\left(\frac{a}{8},\frac{b}{8},h\right)$

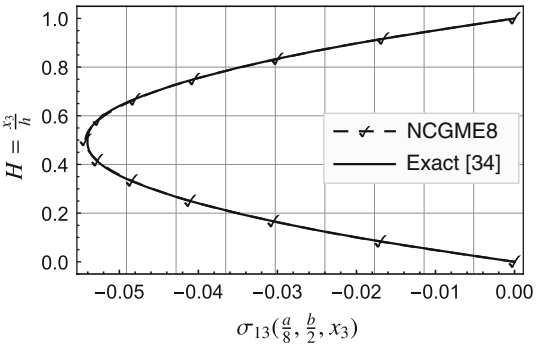

Fig. 11 Distribution along thickness of $\sigma_{13}\left(\frac{a}{8},\frac{b}{2},x_3\right)$

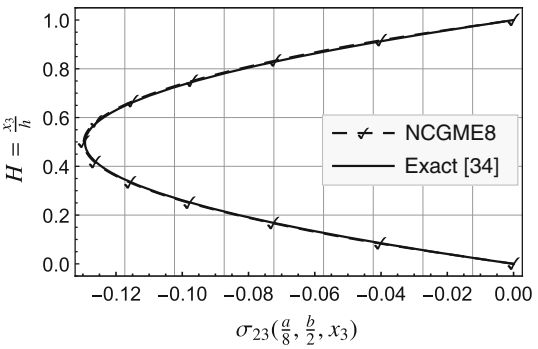

Fig. 12 Distribution along thickness of $\sigma_{23}\left(\frac{a}{8},\frac{b}{2},x_3\right)$

Table 1 Mesh sizes

Mesh size	2×2	3×3	4×4	$\cdots$	11×11	12×12
Mesh number	2	3	4	$\cdots$	11	12

Figures 2–4 show that the results for $u_1\left(\frac{a}{8},\frac{b}{2},h\right)$, $u_2\left(\frac{a}{2},\frac{b}{8},h\right)$, and $u_3\left(\frac{a}{2},\frac{b}{2},\frac{h}{2}\right)$ using NCGME8 were more accurate than those obtained using NCDE8. Their convergence rate was also faster compared with NCDE8.

It is obvious that the results for $\sigma_{13}\left(\frac{a}{8},\frac{b}{2},\frac{h}{2}\right)$ and $\sigma_{23}\left(\frac{a}{2},\frac{b}{8},\frac{h}{2}\right)$ obtained using NCGME8 were in good agreement with the exact solution when the mesh was relatively fine (Figs. 5 and 6). It can also be seen that the accuracy of $\sigma_{13}\left(\frac{a}{8},\frac{b}{2},\frac{h}{2}\right)$ and $\sigma_{23}\left(\frac{a}{2},\frac{b}{8},\frac{h}{2}\right)$ obtained using CGME8 was also greatly superior to that obtained using NCDE8. Generally, displacement methods cannot accurately predict transversal stresses on the neutral plane of a plate, since the along-thickness distribution of σ_{13} and σ_{23} is parabolic, and the maximum or minimum values of σ_{13} and σ_{23} are near to the neutral plane (see Figs. 11 and 12).

Figure 7 shows that the accuracy of $\sigma_{33}\left(\frac{a}{2},\frac{b}{2},h\right)$ obtained using NCDE8 was very poor. As pointed out above, it is difficult to introduce traction boundary conditions when stress variables are computed using constitutive relations at element level. Hence, the stress results obtained using NCDE8 on the boundary are inconsistent with the prescribed stresses. However, the stress results obtained using CGME8 and NCGME8 on the boundary were fully consistent with the prescribed stresses.

The in-plane stress $\sigma_{22}\left(\frac{a}{2},\frac{b}{2},0\right)$ obtained using NCGME8 was characterized by rapid convergence. The convergence rate of $\sigma_{11}\left(\frac{a}{2},\frac{b}{2},0\right)$ and $\sigma_{12}\left(\frac{a}{8},\frac{b}{8},h\right)$ using NCGME8 was also faster than for NCDE8 (Figs. 8 and 10).

Figures 11 and 12 show further that the distribution along thickness of $\sigma_{13}\left(\frac{a}{8},\frac{b}{2},x_3\right)$ and $\sigma_{23}\left(\frac{a}{2},\frac{b}{8},x_3\right)$ obtained using NCGME8 was close to the exact solutions for the $12\times12\times4$ mesh.

5.2 A classical cantilever beam problem

Consider a cantilever beam [35] under pure bending or acted upon by shear forces at the tip (Fig. 13a, b), with geometric dimensions of $2\times2\times10$ and material properties of $E=1500$ and $\nu=0.25$. The vertical displacement at point A and the bending stress σ_{11} at point B for different meshes (as shown in Figs. 14–19) are presented in Tables 2–4, respectively, compared with $Q_{S_{11-1}}$ [35], $Q_{S_{11-2}}$ [35], and exact solutions.

Based on the results in Tables 2–5, it can be concluded that:

Most of the displacement and stress results obtained using NCGME8 appear to be more accurate than those

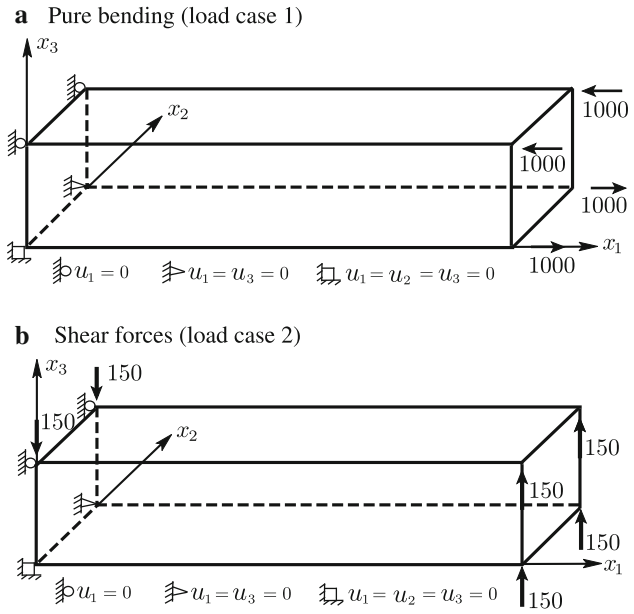

Fig. 13 Two load cases for a cantilever beam

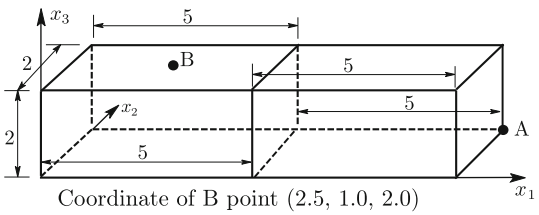

Fig. 14 Mesh a

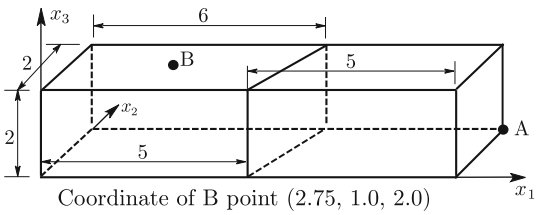

Fig. 15 Mesh b

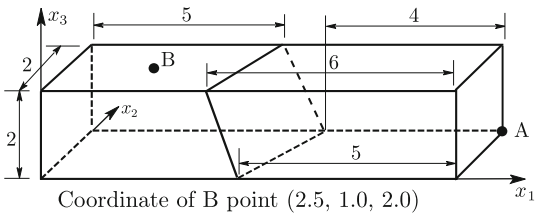

Fig. 16 Mesh c

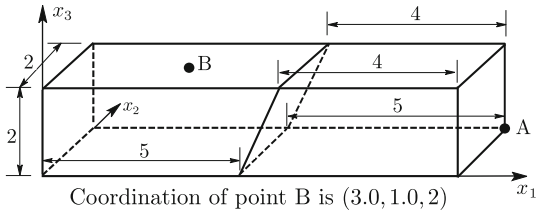

Fig. 17 Mesh d

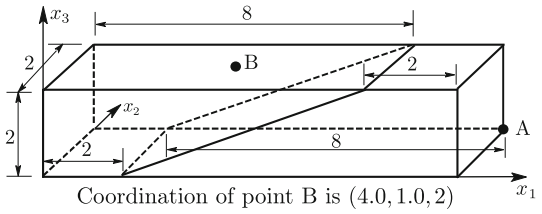

Fig. 18 Mesh e

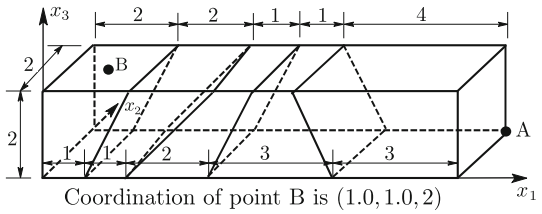

Fig. 19 Mesh f

Table 2 Displacement u_3 at point A (load case 1)

Mesh	QS_{11-1}	QS_{11-2}	CGME8	NCGME8	Exact
a	100.0	100.0	43.5	100.0	100.0
b	89.0	92.2	38.1	97.6	100.0
c	78.8	81.4	33.8	95.9	100.0
d	77.0	77.0	31.4	93.0	100.0
e	31.2	37.5	15.0	75.1	100.0
f	92.2	92.9	60.4	99.6	100.0

Table 3 Stress σ_{11} at point B (load case 1)

Mesh	QS_{11-1}	QS_{11-2}	CGME8	NCGME8	Exact
a	−3000.0	−3000.0	−1304.5	−3000.0	−3000.0
b	−2619.5	−2710.8	−1093.1	−2887.4	−3000.0
c	−2327.2	−2413.1	−936.6	−2795.6	−3000.0
d	−2348.0	−2348.0	−994.8	−2850.1	−3000.0
e	−1162.4	−1380.9	−423.8	−2546.7	−3000.0
f	−3006.6	−3015.1	−2294.9	−2996.5	−3000.0

obtained using the hybrid stress elements QS_{11-1}, QS_{11-2}, and CGME8. NCGME8 is less sensitive to geometric distortions (see Figs. 14–19, in which the elements are severely distorted). It is also very obvious that the accuracy of CGME8 was very poor due to the geometric distortion of the elements.

5.3 Cook's skew beam

Figure 20 shows an arbitrary structure with unit vertical load $\boldsymbol{f}$ uniformly distributed along the right edge with material parameters of $E = 1.0$ and $\nu = \frac{1}{3}$.

Table 4 Displacement u_3 at point A (load case 2)

Mesh	$Q_{S_{11-1}}$	$Q_{S_{11-2}}$	CGME8	NCGME8	Exact
a	96.1	95.9	44.5	101.2	102.6
b	86.5	89.5	40.5	99.8	102.6
c	78.7	81.5	38.8	98.7	102.6
d	78.5	78.4	44.5	98.8	102.6
e	37.4	45.1	22.7	81.8	102.6
f	94.1	94.9	67.6	103.6	102.6

Table 5 Stress σ_{11} at point B (load case 2)

Mesh	$Q_{S_{11-1}}$	$Q_{S_{11-2}}$	CGME8	NCGME8	Exact
a	−3375.0	−3375.0	−1363.9	−3201.8	−3375.0
b	−2925.6	−3024.8	−1122.7	−3025.0	−3262.5
c	−2847.6	−2950.0	−1055.8	−2974.7	−3375.0
d	−2735.0	−2735.7	−1096.8	−2947.2	−3150.0
e	−1623.2	−1935.6	−573.3	−2638.3	−2700.0
f	−4125.3	−4138.2	−3155.8	−4079.0	−4050.0

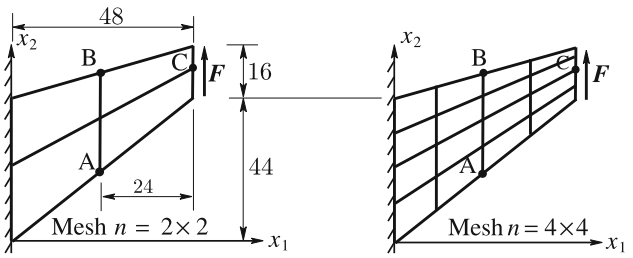

Fig. 20 Cook's skew beam

The numerical results in Table 6 show that NCGME8 was softer than the other elements in Ref. [36]. Without doubt, the results obtained using NCGME8 are closer to the best known answers.

6 Conclusions

Generally, classical mixed methods yield the simplest and most flexible system of equations for finite element analysis of some problems. However, the corresponding mathematical theory is relatively complex due to the requirement for stable elements.

Applying usual linear interpolation functions, two novel and simple generalized mixed elements were developed by combining two variational principles. As mentioned in Sect. 3, one of the most prominent advantages of the generalized mixed methods (GMMs) corresponding to the present mixed elements for the 3D problems presented in this work is that symmetry with respect to both displacement and stress variables is guaranteed in the finite element governing equations. On the other hand, the GMMs are preferable for introduction of displacement and tractions boundary conditions simultaneously. The convergence rates of stress and displacement variables using NCGME8 were balanced, stable, and with fine precision.

Table 6 Results for Cook's skew beam (Fig. 20)

Element	u_2 at C	σ_A	σ_B
Coarse (mesh $n = 2 \times 2$)			
Hybrid, $\lambda = 0.4$ [36]	21.25	0.1736	−0.1737
Hybrid [36], $\lambda = 0.2$ [36]	21.46	0.1772	−0.1811
CST hybrid [36]	21.52	0.1760	−0.1844
CGME8	13.24	0.1108	−0.079
NCGME8	22.80	0.2040	−0.1987
Finer (mesh $n = 4 \times 4$)			
Hybrid, $\lambda = 0.4$ [36]	23.09	0.2130	−0.1768
Hybrid, $\lambda = 0.2$ [36]	23.17	0.2143	−0.1773
CST hybrid [36]	23.17	0.2145	−0.1773
CGME8	19.47	0.2187	−0.1648
NCGME8	23.55	0.2427	−0.1821
Best known answer	23.9	0.236	−0.201

Note: u_2, vertical deflection at C; σ_A, maximum principal stress at A; σ_B, minimum principal stress at B

This noncompatible generalized mixed method should be extended to important applications in a wide range of engineering structures, including treatment of the combination with other structural members and investigation of the possible advantages in stress singularity problems and nonlinear applications which may result for special structures. The pertinent theories of the generalized mixed elements should also be explored deeply, for instance, investigation of local error bounds or practical estimates for variables in three-dimensional problems.

If one starts from the generalized variational principles of plate and shell theories, simple corresponding generalized element formulations and generalized mixed methods can also be constructed.

Acknowledgements This work was supported by the National Natural Science Foundation of China (Grant 11502286).

References

1. Tian, S.Z., Pian, T.H.: Variational Principles with Multi-variables and Finite Elements with Multi-variables. Science Press, Beijing (2011). (in Chinese)
2. Hoa, S.V., Wei, F.: Hybrid Finite Element Method for Stress Analysis of Laminated Composites. Springer Science & Business Media, New York (2013)
3. Herrmann, L.R.: Finite element bending analysis for plates. J. Eng. Mech. Div. ASCE **98**, 13–26 (1967)

4. Brezzi, F.: On the existence, uniqueness and approximation of saddle-point problems arising from lagrangian multipliers. Rev. Fr. Autom. Inf. Rech. Opér. Anal. Numér. **8**, 129–151 (1974)
5. Reddy, J.N., Oden, J.T.: Mathematical theory of mixed finite element approximations. Quart. Appl. Math **33**, 255–280 (1975)
6. Oden, J.T., Reddy, J.N.: On mixed finite element approximations. SIAM J. Numer. Anal. **13**, 393–404 (1976)
7. Strang, G., Fix, G.J.: An Analysis of the Finite Element Method. Prentice-Hall, Englewood Cliffs (1973)
8. Atluri, S.N., Gallagher, R.H., Zienkiewicz, O.C.: Hybrid and Mixed Finite Element Methods. Wiley, New York (1983)
9. Hughes, T.J.: The Finite Element Method: Linear Static and Dynamic Finite Element Analysis. Courier Corporation, North Chelmsford (2012)
10. Morley, M.E.: A family of mixed finite elements for linear elasticity. Numer. Math. **55**, 633–666 (1989)
11. Brezzi, F., Fortin, M.: Mixed and Hybrid Finite Element Methods. Springer Science & Business Media, New York (2012)
12. Belytschko, T., Liu, W.K., Moran, B., et al.: Nonlinear Finite Elements for Continua and Structures. Wiley, New York (2013)
13. Bonet, J., Wood, R.D.: Nonlinear Continuum Mechanics for Finite Element Analysis. Cambridge University Press, London (1997)
14. Zienkiewicz, O.C., Taylor, R.L.: The Finite Element Method: Solid Mechanics. Butterworth, London (2000)
15. Arnold, D.N.: Differential complexes and numerical stability. Preprint. arXiv:math/0212391 (2002)
16. Arnold, D.N., Winther, R.: Mixed finite elements for elasticity. Numer. Math. **92**, 401–419 (2002)
17. Adams, S., Cockburn, B.: A mixed finite element method for elasticity in three dimensions. J. Sci. Comput. **25**, 515–521 (2005)
18. Arnold, D.N., Falk, R., Winther, R.: Mixed finite element methods for linear elasticity with weakly imposed symmetry. Math. Comput. **76**, 1699–1723 (2007)
19. Arnold, D.N., Awanou, G., Winther, R.: Finite elements for symmetric tensors in three dimensions. Math. Comput. **77**, 1229–1251 (2008)
20. Sinwel, A.: A new family of mixed finite elements for elasticity. [Ph.D. Thesis], Johannes Kepler University, Austria (2009)
21. Qiu, W., Demkowicz, L.: Variable order mixed *h*-finite element method for linear elasticity with weakly imposed symmetry. II. Affine and curvilinear elements in 2D. Mathematics **11**, 510–539 (2010)
22. Gopalakrishnan, J., Guzm, J.N.: Symmetric nonconforming mixed finite elements for linear elasticity. SIAM J. Numer. Anal. **49**, 1504–1520 (2011)
23. Qiu, W.: Mixed variable order *h*-finite element method for linear elasticity with weakly imposed symmetry. Curvilinear elements in 2D. Comput. Methods Appl. Math. **11**, 510–539 (2011)
24. Hu, J., Man, H.G., Zhang, S.G.: The simplest mixed finite element method for linear elasticity in the symmetric formulation on *n*-rectangular grids. Comput. Math. Appl. **71**, 1317–1336 (2013)
25. Liu, Z.D.: Basis of Mixed Finite Element Methods and Its Application. Science Press, Beijing (2006). (in Chinese)
26. Arnold, D.N.: Mixed finite element methods for elliptic problems. Comput. Methods Appl. Mech. Eng. **82**, 281–300 (1990)
27. Reissner, E.: On a variational theorem in elasticity. J. Math. Phys. **29**, 90–95 (1950)
28. Chien, W.Z.: Method of high-order lagrange multiplier and generalized variational principles of elasticity with more general forms of functionals. Appl. Math. Mech. **4**, 143–157 (1983)
29. Felippa, C.A.: Parameterized multifid variational principles in elasticity: I. Mixed functionals. Commun. Appl. Numer. Methods **5**, 79–88 (1989)
30. Felippa, C.A.: Parametrized multifid variational principles in elasticity: II. Hybrid functionals and the free formulation. Commun. Appl. Numer. Methods **5**, 89–98 (1989)
31. Zhong, W.X.: Force, Work, Energy and Symplectic Mathematics. Dalian University of Technology Press, Dalian (2007). (in Chinese)
32. Chen, W.J.: A high preccision eight-node hexahedron element. Chin. J. Theor. Appl. Mech. **10**, 1211–1219 (1976)
33. Taylor, R.L., Beresford, P.J., Wilson, E.L.: A non-conforming element for stress analysis. Int. J. Numer. Methods Eng. **10**, 1211–1219 (1976)
34. Fan, J.R.: Exact Theory of Laminated Thick Plates and Shells. Science Press, Beijing (1996). (in Chinese)
35. Cheung, Y.K., Chen, W.J.: Isoparametric hybrid hexahedral elements for 3-D stress analysis. Int. J. Numer. Methods Eng. **26**, 677–693 (1988)
36. Cook, R.D.: A plane hybrid element with rotational DOF and adjustable stiffness. Int. J. Numer. Methods Eng. **24**, 1499–1508 (1987)